Parameter-free retrieval of subcycle asymmetry of polar molecules by high-order harmonic spectroscopy

Kim-Ngan H. Nguyen [1,2,3] Ngoc-Loan Phan [4,*] Cam-Tu Le [5,6,†] DinhDuy Vu [4] and Van-Hoang Le [4]

[1]*Institute of Fundamental and Applied Sciences, Duy Tan University, Ho Chi Minh City 71008, Vietnam*

[2]*Faculty of Natural Sciences, Duy Tan University, Da Nang City 50000, Vietnam*

[3]*Nuclear Training Center, VINATOM, Hanoi 10000, Vietnam*

[4]*Computational Physics Laboratory K002, Department of Physics, Ho Chi Minh City University of Education, Ho Chi Minh City 72711, Vietnam*

[5]*Atomic Molecular and Optical Physics Research Group, Advanced Institute of Materials Science, Ton Duc Thang University, Ho Chi Minh City 72915, Vietnam*

[6]*Faculty of Applied Sciences, Ton Duc Thang University, Ho Chi Minh City 72915, Vietnam*

(Received 16 August 2022; accepted 22 November 2022; published 22 December 2022)

Retrieving atomic and molecular properties from entangling macroscopic measurements is an ambitious task. In particular, the phase difference between the adjacent attosecond bursts emitted from polar molecules is of interest and has been reconstructed from measured high-order harmonic generation (HHG) when molecules are exposed to an intense laser pulse. However, besides the ratio of intensities between the even and odd harmonic orders which can be measured directly, the suggested construction method requires nonmeasured parameters that can be supplied through theoretical calculations. The complexity or comprehensiveness of this theory clearly affects the accuracy of the retrieval procedure. In this study we propose a robust parameter-free method to retrieve the subtle molecular asymmetry, i.e., both the spectral phase difference and intensity ratio of two adjacent attosecond bursts, from purely experimental measurements of HHG. For this purpose, we first figure out that the phase difference is an intrinsic feature of polar molecules, almost independent of the external laser's parameters. After that, we design a detailed procedure to quantitatively extract these features via the time-frequency profile from the intensity and phase measurements of HHG emitted from partially oriented molecular samples. In this step, we develop the analytical formula to convert the phase difference and intensity ratio of a partially oriented sample to those of a single molecule. The accuracy and robustness of the methods are validated by numerical data.

DOI: 10.1103/PhysRevA.106.063108

I. INTRODUCTION

Advances in intense ultrashort laser technologies have facilitated unprecedented nonlinear laser-matter interactions, in which high-order harmonic generation (HHG) is a powerful tool to uncover the structure and dynamics of atoms, molecules, and solids [1–3]. From HHG, one can efficiently synthesize attosecond pulse trains and single attosecond pulses [4,5], leading to breakthroughs in understanding attosecond electron dynamics [6–9]. The HHG emission can be intuitively understood by the semiclassical three-step model where an electron tunneling out of the laser-distorted atomic or molecular potential recombines into the parent ion after being driven in the continuum by the intense laser field [10,11]. In the last step, the accumulated electron kinetic energy is converted into the energy of emitted high-harmonic photons.

High-order harmonic generation is a subtle sub-optical-cycle process. In particular, in a periodic linearly polarized laser, the electron wave packet alternatively collides with opposite sides of the targets, leading to the emission of adjacent attosecond bursts with the time spacing of half the optical cycle of the driving pulse. For atoms and symmetric molecules in a multicycle-driving laser pulse, the amplitude and phase of attosecond pulses do not differ from each other (except for the π change) because of the symmetry (half-period time translation combined with spatial inversion) of the laser-target system. However, in the few-cycle regime with fast modulation of the electric field or in the presence of a weak field, there are a relative phase change and different amplitudes between the adjacent attosecond bursts due to the symmetry breaking. Fully characterizing and controlling these temporal profiles and relative phase changes are crucial for studying the ultrafast phenomena [6,12–14]. For example, by manipulating the temporal interferometer via the relative phases between consecutive attosecond bursts emitted from atoms in a combination of strong driving and weak laser fields, the electric wave function during the field-induced tunneling has been probed [6]. In addition, by controlling the phase of an attosecond-burst train, one can generate extreme ultraviolet (XUV) continua through adjustment of the focus position, infrared (IR) pulse chirp, and carrier-envelope phase [15]. Furthermore, the phases characterized at emission time are

*Corresponding author: loanptn@hcmue.edu.vn

†lethicamtu@tdtu.edu.vn

called dynamical phases, and their relative phase is particularly indispensable in understanding the dynamical origin of harmonics [16,17] and more recently of near- and below-threshold harmonic regimes [18–20].

Regarding linear polar molecules which have the head-versus-tail form with different atoms at the two sides, the electron recombination causes emissions of distinguishable attosecond bursts with half-cycle time spacing [21,22]. These distinctions between the adjacent attosecond bursts manifesting in their phases and amplitudes leave a hint of subcycle asymmetry of a polar molecule in the HHG measurement. The dynamical asymmetries cause the appearance of even harmonics [23,24] and the shape resonance in HHG from polar molecules [25,26].

With recent achievements in molecular-orientation techniques, the phase-matching HHG from highly oriented polar molecules has been experimentally observed with well-resolved odd and even harmonic orders [23,25–29]. Based on this, Frumker *et al.* suggested a way to access the polar-molecular dynamical asymmetry within a subcycle timescale besides the conventional ways of measuring the ionization rate [30–34]. In particular, the phase difference between consecutive attosecond bursts of CO molecules has been experimentally probed via the measured even-to-odd ratio, i.e., the ratio of intensities between the even harmonic orders and the average of the two adjacent odd harmonic orders [23]. However, the theoretical calculation of this phase difference is not available yet.

Besides the measurement input, the method suggested in Ref. [23] needs two parameters: the intensity ratio of two adjacent attosecond bursts and the degrees of orientation. The former is preestimated by an approximate model associated with the amplitude of the recombination dipole and the asymmetry in ionization rate. Moreover, the retrieval formula produces results with a sign ambiguity (plus versus minus), and choosing which one is again based on its theoretical initial estimation. As a result, the precision of the extracted phase difference between the consecutive attosecond bursts significantly depends on the theory level and also on the estimation of the CO ionization rate. Indeed, the accuracy of theoretical models for computing the ionization rate of CO molecules was intensively discussed in recent studies since the multielectron polarization effect may lead to conflicting behaviors compared to the case without this effect [30–34]. Also, the critical role of the multielectron polarization effect in different features of HHG from CO molecules recently revealed [24,35–37]. Our recent study is complementary to the inclusion of the multielectron polarization which makes the simulated even-to-odd ratio fairly match the experimental data [24]. The role of the Stark correction in strong-field phenomena is also a topic of debate [23,25,26,33]. For these reasons, it is desirable for a purely experimental method without any additional theoretical parameters to extract the subcycle asymmetry, particularly the spectral phase difference and intensity ratio between consecutive attosecond bursts.

On the other hand, the time-frequency spectrogram is a specialized method to visualize classical electron trajectories responsible for the emission of HHG. It is a powerful tool for studying electron dynamics during HHG in atomic and molecular systems [24,38–43] and solids [44,45]. Recently, we exploited the time-frequency spectrogram for general characterization of the degrees of orientation of polar molecules [46,47]. Although most applications in electron dynamics of the time-frequency spectrogram are based on its amplitude, the phase of time profiles, i.e., the dynamical phase, is also important since it encodes the interference of the short and long electron trajectories, or of trajectories in each half optical cycle [11,48,49], and it also embeds dynamical origins of harmonics in near- or below-threshold regimes [16–20]. Both the amplitude and phase of the time-frequency profile can be experimentally reconstructed from spectral HHG intensities and phases, which are commonly measured by recent advanced techniques, such as the reconstruction of attosecond beating by interference of two-photon transitions (RABBIT) [50–53] or frequency-resolved optical gating for complete reconstruction of attosecond bursts (FROG-CRAB) [14,54]. More recently, a direct reconstruction of the time-frequency profile by HHG intensity through a time-delay probe XUV pulse has been suggested [55]. The question is whether the reconstructed time-frequency spectrogram can be utilized to extract the phase difference between the two adjacent attosecond bursts.

Our goal is to propose a theoretical base for a promising experimental method to retrieve the subtle subcycle molecular asymmetry, in particular both the phase difference and the intensity ratio between two consecutive attosecond bursts of polar molecules from purely experimental measurements. Before this task, we first simulate the spectral phase difference and intensity ratio between adjacent attosecond bursts emitted from CO molecules in the linearly polarized intense laser pulse by numerically solving the three-dimensional time-dependent Schrödinger equation (TDSE). We also investigate the response of these quantities to the changing of the external laser field to prove the insensitivity of the phase difference to the external laser so that it characterizes the intrinsic properties of polar molecules. This affirmation stimulates the second task to propose a method to retrieve the phase difference and intensity ratio from the time-frequency spectrogram reconstructed by HHG measurements incorporating real experimental conditions: HHG measurement errors, partial orientation, and partial alignment of a molecular sample. The accuracy of the proposed method is examined. Because the required measurement data of the spectral intensity and phase of HHG emitted from polar molecules are not readily available, we generate numerically data by the numerical TDSE method. The macroscopic phase-matching condition is artificially included. The CO molecule is chosen as a representative case of polar molecules.

The rest of the paper is organized as follows. In the next section we briefly present the TDSE method to simulate HHG and the time-frequency profile. Section III is divided into two subsections dealing with the two tasks mentioned above. A summary is given in Sec. IV.

II. NUMERICAL METHODS FOR CALCULATING HHG AND THE TIME-FREQUENCY PROFILE

The procedure of the method for numerically solving the three-dimensional time-dependent Schrödinger equation (the TDSE method) is described in detail in our previous works

(see Ref. [36] for example). Here we briefly recall some main points. The TDSE has the following form in atomic units ($\hbar = m_e = e = 1$):

$$i\frac{\partial}{\partial t}\Psi(\mathbf{r},t) = [\hat{H}_0 + V(\mathbf{r},t)]\Psi(\mathbf{r},t). \tag{1}$$

Here $\hat{H}_0$ is the field-free Hamiltonian of the CO molecule in which the potential of the CO molecule is constructed by the single-active-electron approximation where the outermost electron moves in the effective potential of the nuclei and frozen core electrons [56–58]. To get the molecular wave functions with correct asymptotic behavior, we apply the LB94 model proposed by van Leeuwen and Baerends [56], in which the empirical parameters are chosen to obtain that the energy and permanent dipole of the 5σ orbital are -0.510 and 1.55 a.u., respectively. They match well the values of -0.514 a.u., obtained by experiment [59], and of 1.57 a.u., calculated by the time-dependent density-functional theory [60], respectively.

In the length gauge, the time-dependent potential $V(\mathbf{r},t)$ describes the coupling of the active electron and electric field

$$V(\mathbf{r},t) = \mathbf{r}\cdot\mathbf{E}(t), \tag{2}$$

where the electric field is

$$\mathbf{E}(t) = -\mathbf{e}f(t)E_0\sin(\omega_0 t + \phi). \tag{3}$$

Here E_0, ω_0, ϕ, and $f(t)$ are the peak amplitude, carrier frequency, carrier-envelope phase, and envelope function of a laser pulse, respectively, and $\mathbf{e}$ is a unit vector indicating the polarization of the electric field. The angle between this vector $\mathbf{e}$ and the molecular axis is called the molecular orientation angle β.

Recently, many studies have demonstrated that multielectron polarization is needed for HHG simulation, especially for CO molecules [24,35–37]. Therefore, we include a polarization potential indicating the interaction between the active electron with the laser-induced dynamic core-electron polarization [32,61], which has the form

$$V_{\mathrm{P}}(\mathbf{r},t) = -\frac{\mathbf{E}(t)\hat{\alpha}_c\mathbf{r}}{r^3}, \tag{4}$$

where $\hat{\alpha}_c$ is the total polarization tensor of the core electrons whose components for the CO molecule are $\alpha_{cxx} = \alpha_{cyy} = 6.72$ a.u. and $\alpha_{czz} = 12.22$ a.u. [33]. It is noted that at a small distance near the core, $r \leqslant r_c$ with $r_{cx} = r_{cy} = \alpha_{cxx}^{1/3}$ and $r_{cz} = \alpha_{czz}^{1/3}$, the external electric field and the polarization field cancel each other to avoid the singularity and minimize the unphysical dipole coupling between the highest occupied molecular orbital and the lower ones [34].

The time-dependent wave function $\psi(\mathbf{r},t)$ is obtained by applying the TDSE method presented in Ref. [36]. After getting $\psi(\mathbf{r},t)$, we calculate the time-dependent induced acceleration dipole as

$$\mathbf{a}(t) = \frac{d^2}{dt^2}\langle\psi(\mathbf{r},t)|\mathbf{r}|\psi(\mathbf{r},t)\rangle. \tag{5}$$

For an imperfectly oriented molecular ensemble, the induced acceleration dipole is coherently averaged

$$\mathbf{a}(t) = P_1\mathbf{a}_1(t) + P_2\mathbf{a}_2(t), \tag{6}$$

where P_1 and P_2 are the probabilities of molecules pointing up and down, respectively, along the laser's polarization and $\mathbf{a}_1(t)$ and $\mathbf{a}_2(t)$ are their corresponding time-dependent acceleration dipoles, calculated by Eq. (5).

The Fourier transform of this acceleration dipole gives the amplitude and phase of harmonics with frequency Ω as

$$A(\Omega) = \int_0^\tau a(t)e^{i\Omega t}dt. \tag{7}$$

Here τ is the time duration of the external laser pulse and $a(t) = \hat{\mathbf{n}}\cdot\mathbf{a}(t)$ is the project of the acceleration dipole on a unit vector $\hat{\mathbf{n}}$, which indicates the polarization direction of HHG. The HHG spectrum is the square modulus of $A(\Omega)$ and the HHG phase is the phase of $A(\Omega)$.

The time-frequency spectrogram reveals the spectral and temporal behavior of HHG. It can be accessed through the time-frequency transform, such as the Gabor transform of the induced acceleration dipole

$$A(\Omega,t) = \int dt' a(t')\frac{\exp[-(t'-t)^2/2\sigma^2]}{\sigma\sqrt{2\pi}}\exp(i\Omega t'), \tag{8}$$

where the window width σ controls the temporal-frequency resolutions and $A(\Omega,t)$ encodes both the amplitude and phase of the time-frequency profile.

For numerical convergence, the simulated parameters are taken from our recent work [24] within a spherical box of 100 a.u. with 380 radial grid points, 180 B-spline functions, and 50 partial waves. The time step is 0.055 a.u. The total basis set is 395 213. To avoid the artificial reflection from the grid boundary of the simulated box, the $\cos^{1/8}$ mask function [62] is implemented beyond r_{mask}. The value of $r_{\mathrm{mask}} = 60$ a.u. is set to cover the contribution of both short and long electron trajectories. To keep only the short trajectories, the absorbing boundary is restricted at the maximal displacement of the short trajectories of an electron in the electric field, $r_{\mathrm{mask}} = 1.2E_0/\omega_0^2$ [63–66].

III. RESULTS AND DISCUSSION

A. Intrinsic feature of the phase difference between adjacent attosecond bursts

We assume that CO molecules are perfectly oriented with orientation angle $\beta = 0^\circ$. In this case, only HHG whose polarization parallel to the electric field exists, whereas the HHG with perpendicular polarization evanesces. In this section, based on the solution from the TDSE, we study theoretically the general features of the phase difference and intensity ratio between adjacent attosecond bursts. First, we present the determination of these quantities from the time-frequency spectrogram. Then we investigate their response to the external laser pulse with varying parameters.

1. Simulation of phase difference and intensity imbalance

To ensure the asymmetry of the time profile is contributed by the polar molecule only, the laser pulse duration has to be long enough so that the laser field approximately repeats its magnitude (but in the opposite direction) after every half cycle. For this purpose, we use a ten-cycle laser pulse with a trapezoidal envelope with eight cycles in the flat part and

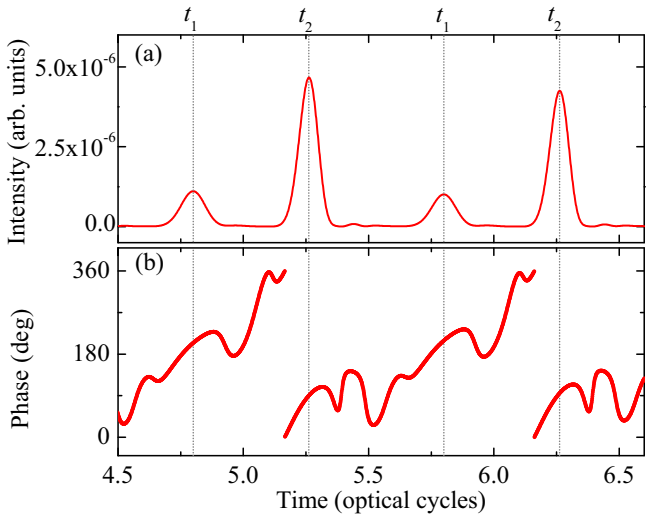

FIG. 1. (a) Time-profile intensity and (b) phase for harmonic order 22 obtained from the Gabor transform (8) with the induced acceleration dipole calculated directly by the TDSE method for CO molecule. The ten-cycle trapezoidal laser pulse with an intensity of 1.5×10^{14} W/cm^2 and wavelength of 800 nm is used. The vertical gray dotted lines indicate the 22nd-order emission instants t_1 and t_2.

two cycles turning up and down. The carrier-envelope phase is 0°. A laser pulse with an intensity of 1.5×10^{14} W/cm^2 and wavelength of 800 nm is used. In this subsection, only the short electron trajectories are selected. The inclusion of longer trajectories will be discussed in detail in the next subsection.

By applying the TDSE method for the interaction of the CO molecule with an intense laser pulse, we obtain the time-dependent wave function, which in turn is used to calculate the time-dependent induced acceleration dipole (5). We then gain the temporal-spectral profile through the Gabor transform (8). As a demonstration, the calculated intensity and phase of the time profile at harmonic order 22 are presented in Fig. 1. It shows that the time profile is revealed as a train of attosecond bursts emitting each half of an optical cycle of the driving laser. The HHG spectrum is formed by the coherent interference of these attosecond bursts. It should be noted that, contrary to the case of atoms or symmetric molecules in which the emission periodicity of the time profile is half of an optical cycle, for a polar molecule such as CO, its periodicity is twice (equal to one optical cycle), which is consistent with the conclusions in Refs. [21,22]. Indeed, the asymmetric nature of a polar molecule breaks the subcycle symmetry, i.e., the half-cycle time translations combined with spatial inversion, leading to the difference between the two adjacent attosecond bursts emitted with half-cycle time spacing, in aspects of both intensity [Fig. 1(a)] and phase [Fig. 1(b)]. Thus, this subcycle asymmetry is attributed to the intrinsic feature of a polar molecule.

To determine the phase difference and intensity ratio between the adjacent attosecond bursts, the first step is specifying their emission instants by looking at the intensity of the time profile for each harmonic order N. Figure 1(a) indicates that, the 22nd harmonic order emits at $t_1 \approx (0.80 + k) \times T_0$ and $t_2 \approx (1.26 + k) \times T_0$, where $k = 4, 5$ and T_0 is an optical period. In the whole scenario, $k = 2, 3, \ldots, 7$ for the ten-cycle laser pulse used. In the next step, the intensities S_1 and S_2 and phases φ_1 and φ_2 of the time profile at these emission instants are defined numerically.

It should be noted that the phase difference between the two adjacent attosecond bursts is defined as usual by

$$\Delta\varphi(N) = \varphi_2(N) - \varphi_1(N) \tag{9a}$$

only for the odd order N, but it needs to add π for the case of even order N as

$$\Delta\varphi(N) = \varphi_2(N) - \varphi_1(N) - \pi. \tag{9b}$$

The reason is the following. The emissions of the two adjacent attosecond bursts are from opposite sides of the polar molecule. As a consequence, the spectral amplitude $A(N)$, coherently synthesized from adjacent attosecond bursts (with half-cycle time spacing) with complex amplitudes $A_1(N)$ and $A_2(N)$, is defined by the formula

$$\begin{aligned} A(N) &= A_1(N) - A_2(N)e^{-iN\omega_0 T_0/2} \\ &\equiv A_1(N) + A_2(N)e^{-i(N+1)\pi}. \end{aligned} \tag{10}$$

This formula clearly clarifies the additional phase π that appears for even harmonics. For further explanation, see Ref. [23].

In a previous study [23], the spectral intensity ratio between the two attosecond bursts was

$$r(N) = \frac{S_2(N)}{S_1(N)} \equiv \frac{|A_2(N)|^2}{|A_1(N)|^2}. \tag{11}$$

However, this intensity ratio has a relatively large range of values which may be hard to control. Therefore, we define instead an alternative quantity called the intensity imbalance as

$$\kappa(N) = \frac{2\sqrt{r(N)}}{1 + r(N)}, \tag{12}$$

whose value is in the range [0,1]. The lower limit implies the maximum asymmetry in intensity between the two adjacent attosecond bursts. Meanwhile, the upper limit characterizes their identical intensity.

The calculation of the intensity imbalance and phase difference is based on the time-frequency transform, whose temporal and frequency resolutions cannot be achieved simultaneously due to the Heisenberg uncertainty principle. The selection of the time-frequency form and its smooth window is essential to balance the temporal and frequency resolutions; thus, it may change the absolute value of the calculated quantities. However, since the intensity imbalance and phase difference between adjacent attosecond bursts are the relative quantities, their values are negligibly affected by changing the time-frequency transform's smooth window function as long as it balances the temporal and frequency resolutions. Our test indicates that varying the window width of the Gabor transform from 5.5 a.u. to 12 a.u. gives stable intensity imbalance and phase difference with the fluctuation characterized by the standard deviation which do not exceed 13% and 11% of means, respectively. Moreover, employing a different transform such as a wavelet transform [16] gives similar values to those obtained by varying the window factor $\xi = \sigma\Omega$ within [7,10] a.u. If the window parameters are

larger than these ranges, the intensity imbalance and phase difference do not change much, but the temporal resolution for some low harmonics is not so good, leading to difficulty in defining their emission times. Throughout this paper, we choose $\sigma = (3\omega_0)^{-1}$ as used in Ref. [39].

The simulated intensity imbalance and phase difference between the two attosecond bursts emitted around $4.80T_0$ and $5.26T_0$ are shown in Fig. 2. The calculation for the other couple of attosecond bursts gives similar results. Figure 2(a) shows a small intensity imbalance corresponding to strong intensity asymmetry occurring for most harmonics except the orders 17–26. For the phase difference exhibited in Fig. 2(b), with increasing harmonic order, the phase difference monotonically decreases after undergoing a turning point around the 20th order where $\Delta\varphi = 90^\circ$, reaches a minimum around order 28, and is followed by an increase.

In Ref. [23] the phase difference was extracted from the measured even-to-odd spectral ratio $E(N)$ by the formula

$$\Delta\varphi_{\text{expt}}(N) \simeq \pm \arccos\left[\frac{1+r(N)}{2\sqrt{r(N)}}\left(1-\frac{2E(N)}{E(N)+\eta^2}\right)\right], \tag{13}$$

where $E(N)$ is defined as the spectral even-to-odd ratio. We note that only the spectral even-to-odd ratio in Eq. (13) is a measured quantity. The other parameters, i.e., the intensity ratio $r(N)$ and degree of orientation η, are estimated theoretically.

In Fig. 2(b) we also show the results obtained in Ref. [23] by red up triangles. These results are comparable to those in the present study for the harmonic-order range from 16 to 24. In fact, besides the branch with the monotonic behavior of the phase difference, there always exists the inverse branch [blue down triangles in Fig. 2(b)] since the equation of phase difference is quadratic, as shown in Eq. (13). However, the monotonic branch was chosen in Ref. [23] based on the shape behavior of the phase difference accumulated during propagation and recombination [23], which may not fully reflect the harmonic process due to the omission of the contribution from the ionization step. Therefore, we also show the inverse branch by the blue down triangles in Fig. 2(b). Interestingly, this inverse branch fits better with our simulation and shows a clear minimum around harmonic orders 24–28. However, a dissimilarity still exists between them, whose reasons are interpreted in the following.

For comparison, we indirectly reconstruct the phase difference by applying Eq. (13) but using our even-to-odd ratio and intensity imbalance calculated by the TDSE method. The results presented in Fig. 2(b) by the green curve show two noticeable points. First, the reconstructed spectral phase differences by the analytical formula (13) (green curve) and the directly calculated ones from the TDSE (black curve) are qualitatively consistent. However, there exists some visible quantitative difference because Eq. (13) is only an approximate expression. Therefore, a direct way to extract the phase difference without utilizing an approximation is needed. Second, when comparing the reconstructed phase difference by TDSE data (green curve) with the experimental inverse branch (blue down triangles), we notice that they are consistent, except for a quantitative vertical shift in the low harmonic orders. It should be emphasized that our simulated even-to-odd ratio agrees considerably with the experimentally measured one in Refs. [23,25], as discussed in detail in Ref. [24]. Therefore, the vertical shift is attributed to both the small difference in the even-to-odd ratio and the accuracy level of the calculated intensity ratio between the attosecond bursts. For these reasons, an extraction method for the phase difference independent of the phenomenological theory is essential.

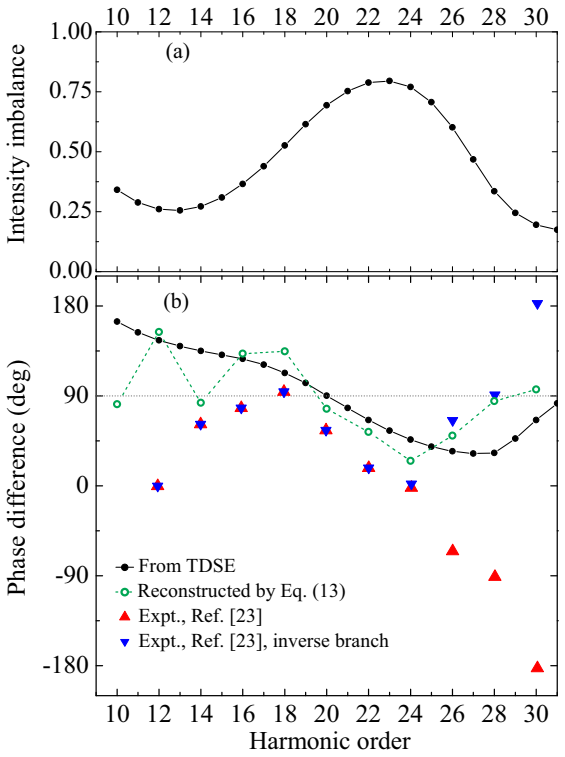

FIG. 2. (a) The HHG spectral intensity imbalance and (b) phase difference between the attosecond bursts emitted around $4.80T_0$ and $5.26T_0$ calculated by the TDSE method (black curve). The horizontal dotted line in (b) shows the phase difference of 90°, at which the turning points are observed. The laser parameters are the same as in Fig. 1. In (b) the reconstruction of the phase difference by Eq. (13), i.e., from the even-to-odd ratio and spectral intensity ratio calculated by the TDSE, is shown (green curve). The experimentally extracted phase difference for monotonic (red triangles) and inverse branches (blue triangles) of Ref. [23] is also presented. Although the tendency of the phase difference theoretically calculated by the TDSE is relatively consistent with the inverse branch, the remaining discrepancy may be attributed to the approximation of the reconstruction equation (13) and the governing of the precalculating quantity in the extraction method in Ref. [23].

2. Stability of the phase difference with changing external laser parameters

The phase difference is considered as a quantity characterizing the subtle intrinsic asymmetry of polar molecules [23]. However, there has been no demonstration of its universal response to the external laser pulse parameters. In previous studies we have shown that the spectral even-to-odd ratio is stable with changing laser parameters if considering only the short electron trajectories [24]. Through this, we believe that

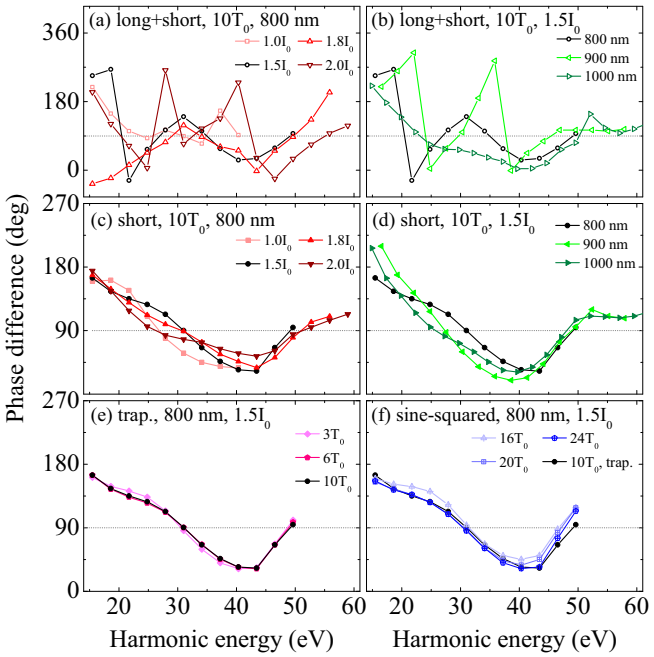

FIG. 3. Spectral phase differences between the adjacent attosecond bursts emitted at instants around $[4.66T_0, 4.95T_0]$ and $[5.14T_0, 5.43T_0]$ when considering [(a) and (b)] both short and long, meanwhile [(c)–(f)] only short trajectories. We used a ten-cycle trapezoidal laser pulse with [(a) and (c)] a wavelength of 800 nm and different intensities and [(b) and (d)] an intensity of 1.5×10^{14} W/cm^2 and different wavelengths. [(e)–(f)] The laser has an intensity of 1.5×10^{14} W/cm^2, wavelength of 800 nm, and (e) a trapezoidal and (f) a sine-squared pulse envelope with varying number of optical cycles. In the legends I_0 denotes 1.0×10^{14} W/cm^2. When filtering long trajectories, the phase difference is stable with diverse laser parameters.

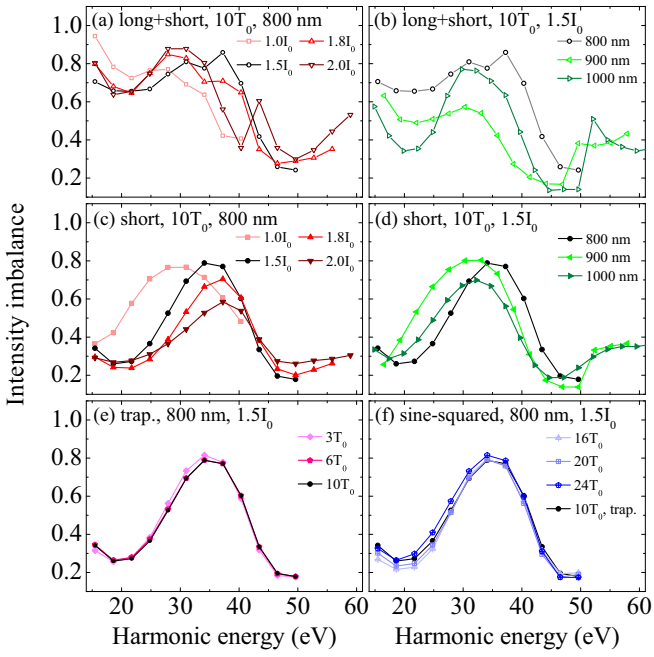

FIG. 4. Same as Fig. 3 but for the intensity imbalance between the adjacent attosecond bursts.

the phase difference is also independent of the external field after removing the long trajectories.

To prove that statement, we study the spectral phase difference and the intensity imbalance between adjacent attosecond bursts in two cases: one keeping both long and short electron trajectories and the other only short trajectories. The latter case theoretically mimics the macroscopic effect in phase-matching experiments with long trajectories being filtered out [63–66]. It should be noted that this phase-matching condition can also be replicated theoretically based on a single-atom response by another approach referred to as intensity coherently averaging, i.e., coherently summing up HHG spectra in a proper range of laser intensity within the laser focus [67–69]. We have examined the calculation of HHG, the phase difference, and the intensity imbalance between two adjacent attosecond bursts by the two approaches of phase-matching mimicry. We recognize that they give similar validity.

The simulated phase difference and intensity imbalance from the TDSE are illustrated in Figs. 3 and 4, respectively. When full electron trajectories are considered [Figs. 3(a), 3(b), 4(a), and 4(b)], the spectral phase difference and intensity imbalance strongly oscillate due to the coherent interference between very close emissions originating from long and short trajectories of the electron's first-order and even higher-order returns in each laser half cycle. This interference can be avoided by absorbing the long trajectories, leading to a smoother variation in the phase differences and intensity imbalances between half-cycle time-spacing attosecond bursts, as shown in Figs. 3(c), 3(d), 4(c), and 4(d).

To continue, we demonstrate in Figs. 3 and 4 the response of the spectral phase difference and intensity imbalance to various laser intensities (but with a fixed wavelength of 800 nm) and laser wavelengths (with a fixed intensity of 1.5×10^{14} W/cm^2). The figures show the two opposite scenarios when including full trajectories [Figs. 3(a), 3(b), 4(a), and 4(b)] and only short trajectories [Figs. 3(c), 3(d), 4(c), and 4(d)]. Indeed, in the former case, the modulation of the spectral phase difference is rapidly fluctuating when varying the laser intensities [Fig. 3(a)] and wavelengths [Fig. 3(b)]. The main features of the phase-difference curves, such as the positions of turning points (where $-\cos\Delta\varphi$ changes from positive to negative [24]) and the minimum, cannot be observed either. On the contrary, in the latter case of removed long trajectories, these curves are apparently stable against an external laser field within the tunneling ionization regime. We also verify the influence of the laser pulse shape on the phase difference, represented in Fig. 3(e) for trapezoidal and in Fig. 3(f) for sine-squared envelopes. We show that the phase difference is independent of the number of optical cycles for a trapezoidal laser pulse [Fig. 3(e)] and for a multicycle sine-squared laser pulse with the number of cycles larger than 16 [Fig. 3(f)]. Moreover, the phase difference when utilizing a multicycle sine-squared pulse is nearly identical to the one of a trapezoidal pulse [Fig. 3(f)].

A similar conclusion is applied for the intensity imbalance between two adjacent attosecond bursts, as shown in Fig. 4. When truncating long trajectories [Figs. 4(c)–4(f)], the spectral intensity imbalance is almost independent of the

laser parameters, including intensities [Fig. 4(c)], wavelengths [Fig. 4(d)], and pulse duration [Figs. 4(e) and 4(f)]; however, the degree of stability here is not as good as for the phase difference, especially when varying the laser intensities. This slight laser dependence may be ascribed to the laser-intensity dependence of the Stark effect in tunneling ionization and in the phase of electron wave-packet propagation for polar molecules [23,25,33,70].

We now explain this stability of the phase difference and intensity imbalance against the changing of laser parameters. Generally, the stability can be understood from the symmetry breaking with respect to the half-period translation. In particular, with the trapezoidal or multicycle sine-squared laser pulses, the magnitude of electric fields is almost unchanged after each half of an optical cycle of the driving laser. Therefore, the only factor that leads to the symmetry breaking resulting in a nonvanishing (or non-π) phase difference is the intrinsic molecular polarization.

For deeper insight, we approach the symmetry breaking in the spirit of the Floquet theorem [37,71]. In a system whose symmetry is broken under the transformation $P:\mathbf{r}\to-\mathbf{r}$, $t\to t+T_0/2$, the induced acceleration dipole can be partitioned as $a(t)=a^g(t)+a^u(t)$, where the gerade (ungerade) component $a^{g(u)}(t)$, satisfying $a^g(t)=+a^g(t+T_0/2)$ and $a^u(t)=-a^u(t+T_0/2)$, couples the wave function with different (similar) parity. Accompanying the definition of the time-frequency transform (8), we can also separate the complex time-frequency signal as $A(\Omega,t)=A^g(\Omega,t)+A^u(\Omega,t)$, with $A^{g(u)}(\Omega,t+T_0/2)=\pm A^{g(u)}(\Omega,t)e^{iN\pi}$. As a consequence, the difference in the phase and amplitude between the adjacent attosecond bursts is embedded in

$$\frac{A(\Omega,t+T_0/2)}{A(\Omega,t)}\equiv\sqrt{r}e^{i\Delta\varphi}=\frac{J-1}{J+1}e^{i(N+1)\pi}, \tag{14}$$

where $J=\frac{A^u(\Omega,t)}{A^g(\Omega,t)}$. Here $A^{g\,(u)}(\Omega,t)$ describes the emission generated as an electron ionizes from and recombines with the components with different (similar) parity of the ground state $|0\rangle$. It is also noted that the gerade component $|0^g\rangle$ of the ground state is mostly responsible for tunneling ionization; therefore, most of the contribution to the $A^{g\,(u)}$ is from an electron ionized from $|0^g\rangle$ which recombines into $|0^{u\,(g)}\rangle$ [37,65,72]. Within the strong-field approximation [11], they can be expressed as $A^{g\,(u)}\approx C\,\langle\mathbf{k}|\hat{\mathbf{n}}\cdot\mathbf{r}|0^g\rangle_i\,\langle 0^{u\,(g)}|\hat{\mathbf{n}}\cdot\mathbf{r}|\mathbf{k}\rangle_r$, where C is the amplitude of the continuum electron, $\mathbf{k}$ characterizes the continuum state, and subindices i and r denote the ionization and recombination steps, respectively. As a result,

$$J=\frac{A^u(\Omega,t)}{A^g(\Omega,t)}\approx\frac{\langle 0^g|\hat{\mathbf{n}}\cdot\mathbf{r}|\mathbf{k}\rangle_r}{\langle 0^u|\hat{\mathbf{n}}\cdot\mathbf{r}|\mathbf{k}\rangle_r} \tag{15}$$

is the ratio between the recombination dipole components representing the transition between the continuum electron wave and the gerade or ungerade parts of ground states. Because J characterizes the target asymmetry only, the difference of time-frequency signal (in both phase and amplitude) between adjacent attosecond bursts [Eq. (14)] has the same behavior, i.e., is stable to the changing of the external laser.

In short, we have demonstrated numerically and proved analytically that the phase difference and intensity imbalance are quantities characterizing the subtle intrinsic asymmetry of polar molecules. Under a phase-matching experimental setup, they are almost unaffected by an external laser pulse.

B. Retrieving the phase difference and intensity imbalance

The preceding section suggested that the phase difference and intensity imbalance are encoded in the time-frequency spectrogram; thus, its reconstruction from measured HHG is completely possible. In fact, the time-frequency profile can be reconstructed from the spectral intensity and phase of HHG, which are currently measurable by advanced techniques [14,50–52,54] or from a direct measurement of time-dependent HHG with time delays of a probe XUV pulse after a pump IR pulse [55]. In this section, first, we present in detail a procedure for a representative of time-frequency reconstruction, i.e., from measured HHG intensity and phase. Here we develop the method to be applied to retrieve the intrinsic molecular properties, i.e., the phase difference and intensity imbalance of a single molecule, from measured HHG of an imperfectly oriented molecular sample. Then we generally apply this procedure and investigate the accuracy of retrieved quantities. The effect of experimental conditions on the method accuracy is discussed.

1. Procedure for retrieving the phase difference and intensity imbalance

(i) First, from the measured HHG intensity $I(\Omega)$ and phase $\Theta(\Omega)$ for different harmonic frequencies Ω, the induced dipole acceleration of the polar molecule can be reconstructed by using the inverse Fourier transform as

$$\breve{a}(t)\propto\sum_{\Omega_i}\sqrt{I(\Omega_i)}e^{i\Theta(\Omega_i)}e^{-i\Omega_i t}. \tag{16}$$

Here Ω_i stands for the discrete harmonic frequency. In fact, this expression is the discrete Fourier transform since the HHG data are practically measured at discrete harmonic orders.

(ii) After that, we apply the time-frequency transform, such as the Gabor transform (8), to get the intensity and phase of the time profile for each harmonic from the induced dipole acceleration (16).

(iii) Then the time-profile intensity of each harmonic is plotted, which shows the emission of a series of attosecond bursts with a time spacing of about a laser half cycle. We find the two adjacent dominant peaks (preferably near the center of the laser pulse to ensure the unchanged laser amplitude after a laser half cycle) and specify their emission instants t_1 and t_2 in the graph.

(iv) At these instants, we determine the intensities S_1 and S_2 and the corresponding phases φ_1 and φ_2 of the two specific adjacent attosecond bursts.

(v) The phase difference and intensity imbalance of these attosecond bursts are defined by Eqs. (9) and (12).

(vi) Since practically no molecular ensemble can be oriented perfectly, the above steps give the extracted quantities for an imperfectly oriented molecular ensemble. Therefore, we have to add a step by developing an expression to obtain the phase difference and intensity imbalance of a single molecule from those of an imperfectly oriented molecular ensemble [Eq. (20)]. Its proof is introduced below.

2. Considering the imperfect orientation of a molecular sample

Practically, the perfect orientation is impossible to achieve experimentally. Generally, a molecular sample after orientation possesses probabilities of molecules pointing up P_1 and down P_2 along with the polarization of a pump pulse. A common quantity characterizing the oriented molecular sample is the degree of orientation defined as $\eta = P_1 - P_2$ whose values range from -1 to 1. Here the two limits $\eta = -1$ and $+1$ stand for the sample whose molecules all point down and up, respectively. To date, molecular degrees of orientation can be measured indirectly by several methods using imaging fragment ion angular distributions after the induced-laser Coulomb explosion [73,74], free-induction decay [75,76], or HHG [23,46,47,77,78]. We recently proposed a simple method to retrieve the degree of orientation from the calibrated time profile reconstructed from measured HHG intensities and phases [46,47].

A natural question is how to detangle the intrinsic polar molecular features, i.e., the phase difference and intensity imbalance of a single molecule, from HHG emitted from an imperfectly oriented molecular sample. Here we figure out the answer by finding an analytical expression describing the connection between the time profiles of the perfectly oriented sample (or, correspondingly, of a single molecule) and an imperfectly oriented sample.

We look thoroughly into an attosecond burst of an imperfectly oriented molecular sample, which has the form

$$W_1 e^{i\Phi_1} \approx P_1 A_1 e^{i\varphi_1} + P_2 A_2 e^{i\varphi_2}, \tag{17}$$

where A_1 and φ_1 stand, respectively, for the amplitude and phase of the attosecond burst from a molecule if it ionizes at the instant when the molecular dipole is parallel to the probe-pulse polarization. In contrast, A_2 and φ_2 are for the antiparallel case. In addition, W_1 and Φ_1 are, respectively, the amplitude and phase of the attosecond burst of an imperfectly oriented molecular sample. Its adjacent attosecond burst emitted after (or before) about half of an optical cycle is written as

$$W_2 e^{i\Phi_2} \approx P_1 A_2 e^{i\varphi_2} + P_2 A_1 e^{i\varphi_1}. \tag{18}$$

The ratio between Eqs. (18) and (17) gives

$$\sqrt{R} e^{i\Delta\Phi} \approx \frac{1 + \zeta\sqrt{r} e^{i\Delta\varphi}}{\zeta + \sqrt{r} e^{i\Delta\varphi}}, \tag{19}$$

where $\zeta = P_1/P_2 \equiv (1+\eta)/(1-\eta)$; $R = |W_2|^2/|W_1|^2$ and $\Delta\Phi = \Phi_2 - \Phi_1$ are, respectively, the intensity ratio and phase difference between the two adjacent attosecond bursts from an imperfectly oriented molecular sample. From this relation we can reconstruct the intensity ratio r and phase difference $\Delta\varphi$ of a single molecule or, in other words, of a perfectly oriented molecular sample, from the ones (R and $\Delta\Phi$) of an imperfectly oriented molecular sample as

$$\sqrt{r} e^{i\Delta\varphi} \approx \frac{\zeta\sqrt{R} e^{i\Delta\Phi} - 1}{\zeta - \sqrt{R} e^{i\Delta\Phi}}. \tag{20}$$

It is worth noting that this expression is definable only when $\zeta \neq 1$ (or $\eta \neq 0$), i.e., the molecular sample has to be oriented before interacting with the probe laser pulse to generate high harmonic spectra.

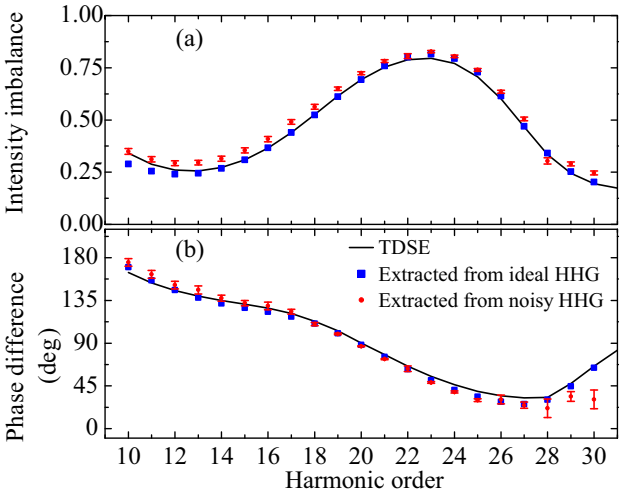

FIG. 5. (a) Spectral intensity imbalance and (b) phase difference extracted from ideal HHG (blue squares) and noisy HHG (red circles). The results are benchmarked with the direct calculations by the TDSE method (black curves). The error bars present the propagated errors with 95% confidence interval for extracted phase differences and intensity imbalances. The laser parameters are the same as in Fig. 1. The extracted information matches the calculated results well.

3. Examining the accuracy of the proposed method

We utilize the numerical HHG intensity and phase simulated by the TDSE method as input data for testing the validation of our proposed method. As discussed in the preceding section, the macroscopic effect is artificially mimicked by keeping short trajectories only. The ten-cycle trapezoidal laser pulse with an intensity of 1.5×10^{14} W/cm^2 and a wavelength of 800 nm is used. In our examination, we assume that the spectral HHG intensity and phase are "measured" within the plateau region at integer harmonic orders, i.e., the step of collected data is one harmonic order.

For this purpose, we benchmark the phase difference and intensity imbalance extracted by the previous procedure, i.e., from Eqs. (16), (8), and (20), with the ones directly calculated from the TDSE method based on Eqs. (6) and (8). We consider step by step how each experimental condition affects the method accuracy.

(a) Examining the systematic error. To examine the systematic error caused by the retrieving method, we first assume that the molecular ensemble is perfectly oriented and apply the above procedure to extract the intensity imbalance and phase difference between adjacent attosecond bursts. The results are exhibited in Fig. 5. It demonstrates that both the extracted intensity imbalance and phase differences (blue squares) are fairly consistent with the ones calculated by the TDSE (black curve) despite the discretization of HHG signals. The average discrepancy between the extracted and calculated data is 3.06% for the intensity imbalances and 5.73% for the phase differences. It is worth noting that it is not required to take the full range of discrete harmonic orders from one to cutoff but only a small window around each specific harmonic order at which asymmetric quantities are needed to extract. Our numerical test shows that a window of about 11 harmonic orders is sufficient to reconstruct the intensity imbalance and

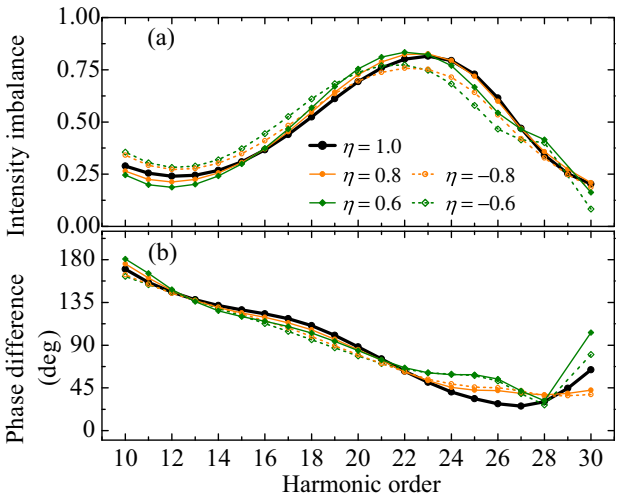

FIG. 6. (a) Reconstruction of single molecular spectral intensity imbalance and (b) phase difference from HHG of imperfectly oriented samples of CO molecules at different degrees of orientation η. The laser parameters are the same as in Fig. 1. The reconstructed results are accurate despite imperfect molecular orientation.

the phase difference with the corresponding average discrepancy between the extracted and calculated data of 8.63% and 11.56%. We conclude that our proposed method is highly reliable for extracting intrinsic asymmetry manifesting via the phase difference and intensity imbalance of polar molecules.

(b) Error propagation from HHG measurements. The above extraction from "ideal" HHG gives the systematic error of the proposed method. In fact, the method's accuracy is also affected by the random errors propagated from the errors of HHG measurement including intensity and phase. To mimic real data of HHG measurement, we prepare "noisy" HHG data by seeding random errors with 95% confidence interval of 40% and 20%, respectively [51], to the HHG intensities and phase of signals simulated from the TDSE. With the same procedure as in Sec. III B 1 applied for these "noisy" HHGs, the extracted intensity imbalances and phase differences together with propagated random errors are exhibited by red circles in Fig. 5. The expected values of extracted information quantitatively match the benchmarked ones with small dispersion despite large random errors of noisy HHG measurements. The propagated errors with a 95% confidence interval for extracted phase differences and intensity imbalances are presented by the error bars as shown in Fig. 5. They are less than 5% except for the phase difference near the spectral minimum. Thus, the proposed method works robustly and reliably with realistic HHG measurement errors.

(c) From a partially oriented molecular sample. To examine the accuracy of the proposed method presented in Sec. III B 1 as a whole, i.e., from a partially oriented molecular sample, we first prepare the numerical HHG for an imperfectly oriented molecular sample using the TDSE method, using Eq. (6). Then we fully apply the proposed procedure to retrieve the intensity ratio r (and also intensity imbalance κ) and phase difference $\Delta\varphi$ of a single molecule from HHG of an imperfectly oriented molecular sample.

Figure 6 demonstrates the reconstruction of single molecular spectral intensity imbalance [Fig. 6(a)] and phase difference [Fig. 6(b)] from "measured" HHG of imperfectly oriented molecular samples at different degrees of orientation. The reconstructed results are fairly consistent with each other despite the imperfect orientation of molecular samples. They also considerably match the curve of $\eta = 1$, i.e., of a single molecule (or a perfectly oriented molecular sample). The averaged discrepancies of reconstructed intensity imbalance from imperfectly and perfectly oriented molecular samples are 6.90% and 6.13% for $\eta = +0.8$ and -0.8, respectively. For the phase differences, these discrepancies are 9.13% and 11.68%. For $\eta = +0.6$ and -0.6, there is an irregular point at harmonic order 29 (not shown) which can be caused by the accidental vanishing of the numerator $\zeta Re^{i\Delta\Phi} - 1$ in Eq. (20), leading to the singular phase difference. This raw error should be eliminated. In short, we conclude that the proposed method effectively validates retrieving the intrinsic asymmetry of a polar molecule via intensity imbalance and phase differences regardless of the imperfect orientation of molecular samples.

(d) Effect of partial molecular alignment. Above, we assumed that the molecules are imperfectly oriented but perfectly aligned along with the pump-pulse polarization. In fact, a number of molecules always deviate from the pump-pulse direction. This necessitates the validation of the proposed method since the detectability of the molecular asymmetry considerably weakens as the alignment angle β increases, i.e., the angle between the molecular axis and probe-pulse polarization.

We investigate the molecular alignment effect on the accuracy of the proposed method by calculating the averaged deviations of extracted phase difference and intensity imbalance from imperfectly aligned molecules compared with those of perfectly oriented ones. For the phase difference, they are 4.89%, 17.75%, and 30.69% for molecular alignment angles $\beta = 10^\circ$, 20°, and 30°, respectively. The deviations for the intensity imbalance are worse: 6.69%, 19.91%, and 37.37%, respectively. Available advanced techniques allow high degrees of molecular alignment, about 0.6–0.8, even above 0.8 [25,74,79], compared with 1 for perfect molecular alignment. With these alignment degrees, for example, 0.8, the percentages of molecules distributed with alignment angles less than 5°, 10°, and 15° are 90.74%, 95.41%, and 96.96%, respectively [80]. In other words, most molecules align within a small alignment angle where our proposed method works reliably. Therefore, with a general experimental setup, the proposed method is sufficiently capable of retrieving the phase difference and intensity imbalance.

In short, to ensure that the retrieved phase difference and intensity imbalance reflect the intrinsic asymmetry of a single polar molecule from HHG emitted from a molecular sample, it is necessary to avoid contaminating the laser effects by using a multicycle (or trapezoidal) laser pulse. In addition, the alignment effect needs to be reduced by preparing a well-aligned molecular sample. Finally, the molecular sample has to be oriented, although perfect orientation is not crucial.

Clearly, different from the method presented in Ref. [23], our proposed procedure does not need the preestimation of any microscopic quantity and just requires the measurements

of the macroscopic quantities: spectral HHG intensity and phase. Therefore, this method allows parameter-free retrieval of the subcycle intrinsic asymmetry, i.e., the phase difference and intensity imbalance of adjacent attosecond bursts of polar molecules.

IV. CONCLUSION

In this paper we have comprehensively studied the properties of the phase difference and intensity imbalance of the polar CO molecule and then proposed a general method to retrieve them from experimental HHG.

First, we provided the theoretical calculation of the phase difference between the consecutive attosecond bursts emitted from the CO molecule. We also compared this theoretical result with the experimental data from a previous study and discussed in detail the consistency and discrepancy between them. Then we numerically demonstrated and analytically proved that the phase difference and intensity imbalance between adjacent attosecond bursts are intrinsic properties characterizing the subcycle molecular asymmetry. In particular, with the good phase-matching HHG experiments, the phase difference is almost independent of the external laser parameters as a consequence of eliminating the quantum path interference of short and long electron trajectories.

Second, we proposed a parameter-free method to retrieve these intrinsic subtle properties, i.e., the spectral phase difference and intensity imbalance, via the time-frequency profile reconstructed from HHG measurements, such as HHG intensity by using a time-delay probe XUV pulse, or spectral HHG intensity and phase. The detailed procedure for the latter approach was presented for a general HHG experiment from a partially oriented molecular sample. Here we derived and justified a relation between the time profiles of a single molecule and those of an imperfectly oriented molecular sample. We proved its effectiveness regardless of the imperfect orientation of molecular samples.

Finally, using numerical data of HHG intensity and phase generated by the TDSE method, we examined the accuracy of the method. The systematic error and the effect of real experimental conditions, including the macroscopic propagation effect, HHG measurement errors, partial molecular alignment, and partial molecular orientation, were discussed. We indicated that the proposed method works robustly and reliably within the general experimental conditions. Our proposal serves as a parameter-free procedure to experimentally obtain the intrinsic asymmetry of polar molecules from HHG. These measured intrinsic properties can be further utilized to characterize the polar molecules or probe their geometrical and dynamic structures.

Since the retrieving method does not require specific conditions for molecular targets, it can be applied to other molecules. Our initial test for linear (NO, CO, and OCS) and complex (CH_4) molecules confirmed the robustness and reliability of the method. Besides demonstrating that the phase difference and intensity imbalance between attosecond bursts are intrinsic properties of molecules, the test also revealed that these extracted quantities reflect the degree of molecular asymmetry.

ACKNOWLEDGMENTS

N.-L.P. and K.-N.H.N. were funded by Ho Chi Minh City University of Education Foundation for Science and Technology under Grant No. CS.2021.19.05TD. K.-N.H.N. was funded by the Master, Ph.D. Scholarship Programme of Vingroup Innovation Foundation (VINIF), Institute of Big Data, Code No. VINIF.2022.TS.078. This work was funded by Vietnam National Foundation for Science and Technology Development (NAFOSTED) under Grant No. 103.01-2020.57. This work was carried out by the high-performance cluster at Ho Chi Minh City University of Education, Vietnam.

[1] F. Krausz and M. Ivanov, Rev. Mod. Phys. **81**, 163 (2009).
[2] S. Ghimire, A. D. DiChiara, E. Sistrunk, P. Agostini, L. F. DiMauro, and D. A. Reis, Nat. Phys. **7**, 138 (2011).
[3] S. Ghimire and D. A. Reis, Nat. Phys. **15**, 10 (2019).
[4] J. Li, X. Ren, Y. Yin, K. Zhao, A. Chew, Y. Cheng, E. Cunningham, Y. Wang, S. Hu, Y. Wu, M. Chini, and Z. Chang, Nat. Commun. **8**, 186 (2017).
[5] T. Gaumnitz, A. Jain, Y. Pertot, M. Huppert, I. Jordan, F. Ardana-Lamas, and H. J. Wörner, Opt. Express **25**, 27506 (2017).
[6] O. Pedatzur, G. Orenstein, V. Serbinenko, H. Soifer, B. Bruner, A. Uzan, D. Brambila, A. Harvey, L. Torlina, F. Morales, O. Smirnova, and N. Dudovich, Nat. Phys. **11**, 815 (2015).
[7] G. Sansone, F. Kelkensberg, J. Pérez-Torres, F. Morales, M. F. Kling, W. Siu, O. Ghafur, P. Johnsson, M. Swoboda, E. Benedetti, F. Ferrari, F. Lépine, J. L. Sanz-Vicario, S. Zherebtsov, I. Znakovskaya, A. L'Huillier, M. Y. Ivanov, M. Nisoli, F. Martín, and M. J. J. Vrakking, Nature (London) **465**, 763 (2010).
[8] R. Locher, L. Castiglioni, M. Lucchini, M. Greif, L. Gallmann, J. Osterwalder, M. Hengsberger, and U. Keller, Optica **2**, 405 (2015).
[9] J. Biegert, F. Calegari, N. Dudovich, F. Quéré, and M. Vrakking, J. Phys. B **54**, 070201 (2021).
[10] P. B. Corkum, Phys. Rev. Lett. **71**, 1994 (1993).
[11] M. Lewenstein, P. Balcou, M. Y. Ivanov, A. L'Huillier, and P. B. Corkum, Phys. Rev. A **49**, 2117 (1994).
[12] C. Guo, A. Harth, S. Carlström, Y.-C. Cheng, S. Mikaelsson, Mårsell, C. Heyl, M. Miranda, M. Gisselbrecht, M. B. Gaarde, K. J. Schafer, A. Mikkelsen, J. Mauritsson, C. L. Arnold, and A. L'Huillier, J. Phys. B **51**, 034006 (2018).
[13] R. López-Martens, K. Varjú, P. Johnsson, J. Mauritsson, Y. Mairesse, P. Salières, M. B. Gaarde, K. J. Schafer, A. Persson, S. Svanberg, C.-G. Wahlström, and A. L'Huillier, Phys. Rev. Lett. **94**, 033001 (2005).

[14] Z. Yang, W. Cao, X. Chen, J. Zhang, Y. Mo, H. Xu, K. Mi, Q. Zhang, P. Lan, and P. Lu, Opt. Lett. **45**, 567 (2020).

[15] W. Holgado, C. Hernández-García, B. Alonso, M. Miranda, F. Silva, L. Plaja, H. Crespo, and I. J. Sola, Phys. Rev. A **93**, 013816 (2016).

[16] X.-M. Tong and S.-I. Chu, Phys. Rev. A **61**, 021802(R) (2000).

[17] J. J. Carrera, X. M. Tong, and S.-I. Chu, Phys. Rev. A **74**, 023404 (2006).

[18] P.-C. Li, Y.-L. Sheu, C. Laughlin, and S.-I. Chu, Nat. Commun. **6**, 7178 (2015).

[19] J. Heslar and S.-I. Chu, Sci. Rep. **6**, 37774 (2016).

[20] L. Han, P.-C. Li, and S.-I. Chu, Laser Phys. Lett. **17**, 115301 (2020).

[21] G. L. Kamta, A. D. Bandrauk, and P. B. Corkum, J. Phys. B **38**, L339 (2005).

[22] P. Lan, P. Lu, W. Cao, X. Wang, and W. Hong, Opt. Lett. **32**, 1186 (2007).

[23] E. Frumker, N. Kajumba, J. B. Bertrand, H. J. Wörner, C. T. Hebeisen, P. Hockett, M. Spanner, S. Patchkovskii, G. G. Paulus, D. M. Villeneuve, A. Naumov, and P. B. Corkum, Phys. Rev. Lett. **109**, 233904 (2012).

[24] H. T. Nguyen, K.-N. H. Nguyen, N.-L. Phan, C.-T. Le, D. Vu, L.-P. Tran, and V.-H. Le, Phys. Rev. A **105**, 023106 (2022).

[25] P. M. Kraus, D. Baykusheva, and H. J. Wörner, Phys. Rev. Lett. **113**, 023001 (2014).

[26] P. M. Kraus, D. Baykusheva, and H. J. Wörner, J. Phys. B **47**, 124030 (2014).

[27] E. Frumker, C. T. Hebeisen, N. Kajumba, J. B. Bertrand, H. J. Wörner, M. Spanner, D. M. Villeneuve, A. Naumov, and P. B. Corkum, Phys. Rev. Lett. **109**, 113901 (2012).

[28] P. M. Kraus, A. Rupenyan, and H. J. Wörner, Phys. Rev. Lett. **109**, 233903 (2012).

[29] P. Kraus, O. I. Tolstikhin, D. Baykusheva, A. Rupenyan, J. Schneider, C. Z. Bisgaard, T. Morishita, F. Jensen, L. B. Madsen, and H. J. Wörner, Nat. Commun. **6**, 7039 (2015).

[30] H. Li, D. Ray, S. De, I. Znakovskaya, W. Cao, G. Laurent, Z. Wang, M. F. Kling, A. T. Le, and C. L. Cocke, Phys. Rev. A **84**, 043429 (2011).

[31] J. Wu, L. P. H. Schmidt, M. Kunitski, M. Meckel, S. Voss, H. Sann, H. Kim, T. Jahnke, A. Czasch, and R. Dörner, Phys. Rev. Lett. **108**, 183001 (2012).

[32] B. Zhang, J. Yuan, and Z. Zhao, Phys. Rev. Lett. **111**, 163001 (2013).

[33] V.-H. Hoang, S.-F. Zhao, V.-H. Le, and A.-T. Le, Phys. Rev. A **95**, 023407 (2017).

[34] M. Abu-samha and L. B. Madsen, Phys. Rev. A **101**, 013433 (2020).

[35] B. Zhang, J. Yuan, and Z. Zhao, Phys. Rev. A **90**, 035402 (2014).

[36] C.-T. Le, V.-H. Hoang, L.-P. Tran, and V.-H. Le, Phys. Rev. A **97**, 043405 (2018).

[37] N.-L. Phan, C.-T. Le, V.-H. Hoang, and V.-H. Le, Phys. Chem. Chem. Phys. **21**, 24177 (2019).

[38] A. Zaïr, M. Holler, A. Guandalini, F. Schapper, J. Biegert, L. Gallmann, U. Keller, A. S. Wyatt, A. Monmayrant, I. A. Walmsley, E. Cormier, T. Auguste, J. P. Caumes, and P. Salières, Phys. Rev. Lett. **100**, 143902 (2008).

[39] C. C. Chirilă, I. Dreissigacker, E. V. van der Zwan, and M. Lein, Phys. Rev. A **81**, 033412 (2010).

[40] Y.-l. Sheu, H.-t. Wu, and L.-Y. Hsu, Opt. Express **23**, 30459 (2015).

[41] N.-L. Phan, K.-N. Do, V.-H. Hoang, C.-T. Le, and V.-H. Le, J. Opt. Soc. Am. B **37**, 1781 (2020).

[42] C. Hernández-García and L. Plaja, Phys. Rev. A **93**, 023402 (2016).

[43] C.-T. Le, N.-L. Phan, D. D. Vu, C. Ngo, and V.-H. Le, Phys. Chem. Chem. Phys. **24**, 6053 (2022).

[44] G. Vampa and T. Brabec, J. Phys. B **50**, 083001 (2017).

[45] T. Ikemachi, Y. Shinohara, T. Sato, J. Yumoto, M. Kuwata-Gonokami, and K. L. Ishikawa, Phys. Rev. A **95**, 043416 (2017).

[46] N.-L. Phan, K.-N. H. Nguyen, C.-T. Le, D. D. Vu, K. Tran, and V.-H. Le, Phys. Rev. A **102**, 063104 (2020).

[47] K.-N. H. Nguyen, N.-L. Phan, C.-T. Le, and D. D. Vu, J. Phys.: Conf. Ser. **1932**, 012003 (2021).

[48] J. Tate, T. Auguste, H. G. Muller, P. Salières, P. Agostini, and L. F. DiMauro, Phys. Rev. Lett. **98**, 013901 (2007).

[49] K. Schiessl, K. L. Ishikawa, E. Persson, and J. Burgdörfer, Phys. Rev. Lett. **99**, 253903 (2007).

[50] P. M. Paul, E. S. Toma, P. Breger, G. Mullot, F. Augé, P. Balcou, H. G. Muller, and P. Agostini, Science **292**, 1689 (2001).

[51] A. Rupenyan, J. B. Bertrand, D. M. Villeneuve, and H. J. Wörner, Phys. Rev. Lett. **108**, 033903 (2012).

[52] J. Mauritsson, P. Johnsson, E. Gustafsson, A. L'Huillier, K. J. Schafer, and M. B. Gaarde, Phys. Rev. Lett. **97**, 013001 (2006).

[53] G. Laurent, W. Cao, H. Li, Z. Wang, I. Ben-Itzhak, and C. L. Cocke, Phys. Rev. Lett. **109**, 083001 (2012).

[54] Y. Mairesse and F. Quéré, Phys. Rev. A **71**, 011401(R) (2005).

[55] T. S. Sarantseva, A. A. Silaev, A. A. Romanov, N. V. Vvedenskii, and M. V. Frolov, Opt. Express **29**, 1428 (2021).

[56] R. van Leeuwen and E. J. Baerends, Phys. Rev. A **49**, 2421 (1994).

[57] M. Abu-samha and L. B. Madsen, Phys. Rev. A **81**, 033416 (2010).

[58] S.-F. Zhao, C. Jin, A.-T. Le, T. F. Jiang, and C. D. Lin, Phys. Rev. A **81**, 033423 (2010).

[59] K. Siegbahn, J. Electron Spectrosc. Relat. Phenom. **5**, 3 (1974).

[60] J. Heslar, D. A. Telnov, and S.-I. Chu, Phys. Rev. A **96**, 063404 (2017).

[61] Z. Zhao and T. Brabec, J. Mod. Opt. **54**, 981 (2007).

[62] H. Yu and A. D. Bandrauk, Phys. Rev. A **56**, 685 (1997).

[63] V. V. Strelkov, M. A. Khokhlova, A. A. Gonoskov, I. A. Gonoskov, and M. Y. Ryabikin, Phys. Rev. A **86**, 013404 (2012).

[64] S. Yu, B. Zhang, Y. Li, S. Yang, and Y. Chen, Phys. Rev. A **90**, 053844 (2014).

[65] B. Zhang, S. Yu, Y. Chen, X. Jiang, and X. Sun, Phys. Rev. A **92**, 053833 (2015).

[66] B. Zhang and M. Lein, Phys. Rev. A **100**, 043401 (2019).

[67] T. Morishita, A.-T. Le, Z. Chen, and C. D. Lin, Phys. Rev. Lett. **100**, 013903 (2008).

[68] A.-T. Le, T. Morishita, and C. D. Lin, Phys. Rev. A **78**, 023814 (2008).

[69] C. Jin, A.-T. Le, and C. D. Lin, Phys. Rev. A **79**, 053413 (2009).

[70] G. L. Kamta and A. D. Bandrauk, Phys. Rev. Lett. **94**, 203003 (2005).

[71] N. Ben-Tal, N. Moiseyev, and A. Beswick, J. Phys. B **26**, 3017 (1993).
[72] Y. Chen and B. Zhang, Phys. Rev. A **84**, 053402 (2011).
[73] H. Sakai, S. Minemoto, H. Nanjo, H. Tanji, and T. Suzuki, Phys. Rev. Lett. **90**, 083001 (2003).
[74] S. De, I. Znakovskaya, D. Ray, F. Anis, N. G. Johnson, I. A. Bocharova, M. Magrakvelidze, B. D. Esry, C. L. Cocke, I. V. Litvinyuk, and M. F. Kling, Phys. Rev. Lett. **103**, 153002 (2009).
[75] S. Fleischer, Y. Zhou, R. W. Field, and K. A. Nelson, Phys. Rev. Lett. **107**, 163603 (2011).
[76] P. Babilotte, K. Hamraoui, F. Billard, E. Hertz, B. Lavorel, O. Faucher, and D. Sugny, Phys. Rev. A **94**, 043403 (2016).
[77] Y. Z. Shi, B. Zhang, W. Y. Li, S. J. Yu, and Y. J. Chen, Phys. Rev. A **95**, 033406 (2017).
[78] S. J. Yu, W. Y. Li, Y. P. Li, and Y. J. Chen, Phys. Rev. A **96**, 013432 (2017).
[79] K. Chordiya, I. Simkó, T. Szidarovszky, and M. U. Kahaly, Sci. Rep. **12**, 8280 (2022).
[80] M. Lein, R. D. Nalda, E. Heesel, N. Hay, E. Springate, R. Velotta, M. Castillejo, P. L. Knight, and J. P. Marangos, J. Mod. Opt. **52**, 465 (2005).